University of Montana
ScholarWorks at University of Montana

Numerical Terradynamic Simulation Group Publications

Numerical Terradynamic Simulation Group

5-2017

Satellite-observed changes in vegetation sensitivities to surface soil moisture and total water storage variations since the 2011 Texas drought

A. Geruo

I. Velicogna

John S. Kimball
University of Montana - Missoula

Jinyang Du
University of Montana - Missoula

Youngwook Kim

See next page for additional authors

Follow this and additional works at: https://scholarworks.umt.edu/ntsg_pubs

Let us know how access to this document benefits you.

Recommended Citation

A. Geruo, I. Velicogna, J. S. Kimball, Jinyang Du, Youngwook Kim, Andreas Colliander, Eni Njoku. (2017) Satellite-observed changes in vegetation sensitivities to surface soil moisture and total water storage variations since the 2011 Texas drought. Environmental Research Letters, 12(5), doi: https://doi.org/10.1088/1748-9326/aa6965

This Article is brought to you for free and open access by the Numerical Terradynamic Simulation Group at ScholarWorks at University of Montana. It has been accepted for inclusion in Numerical Terradynamic Simulation Group Publications by an authorized administrator of ScholarWorks at University of Montana. For more information, please contact scholarworks@mso.umt.edu.

Authors
A. Geruo, I. Velicogna, John S. Kimball, Jinyang Du, Youngwook Kim, Andreas Colliander, and Eni G. Njoku

This article is available at ScholarWorks at University of Montana: https://scholarworks.umt.edu/ntsg_pubs/379

Environmental Research Letters

LETTER

Satellite-observed changes in vegetation sensitivities to surface soil moisture and total water storage variations since the 2011 Texas drought

Geruo A[1,4], Isabella Velicogna[1,2], John S Kimball[3], Jinyang Du[3], Youngwook Kim[3] and Eni Njoku[2]

[1] Department of Earth System Science, University of California Irvine, Irvine, CA, United States of America
[2] Jet Propulsion Laboratory, California Institute of Technology, Pasadena, CA, United States of America
[3] Numerical Terradynamic Simulation Group, College of Forestry & Conservation, University of Montana, Missoula, MT, United States of America
[4] Author to whom any correspondence should be addressed.

E-mail: geruoa@uci.edu

Keywords: drought, terrestrial water storage, soil moisture, remote sensing, solar-induced fluorescence, vegetation-moisture sensitivity

Supplementary material for this article is available online

OPEN ACCESS

RECEIVED
20 June 2016

REVISED
20 March 2017

ACCEPTED FOR PUBLICATION
27 March 2017

PUBLISHED
3 May 2017

Original content from this work may be used under the terms of the Creative Commons Attribution 3.0 licence.

Any further distribution of this work must maintain attribution to the author(s) and the title of the work, journal citation and DOI.

Abstract

We combine soil moisture (SM) data from AMSR-E and AMSR-2, and changes in terrestrial water storage (TWS) from time-variable gravity data from GRACE to delineate and characterize the evolution of drought and its impact on vegetation growth. GRACE-derived TWS provides spatially continuous observations of changes in overall water supply and regional drought extent, persistence and severity, while satellite-derived SM provides enhanced delineation of shallow-depth soil water supply. Together these data provide complementary metrics quantifying available plant water supply. We use these data to investigate the supply changes from water components at different depths in relation to satellite-based enhanced vegetation index (EVI) and gross primary productivity (GPP) from MODIS and solar-induced fluorescence (SIF) from GOME-2, during and following major drought events observed in the state of Texas, USA and its surrounding semiarid area for the past decade. We find that in normal years the spatial pattern of the vegetation–moisture relationship follows the gradient in mean annual precipitation. However since the 2011 hydrological drought, vegetation growth shows enhanced sensitivity to surface SM variations in the grassland area located in central Texas, implying that the grassland, although susceptible to drought, has the capacity for a speedy recovery. Vegetation dependency on TWS weakens in the shrub-dominated west and strengthens in the grassland and forest area spanning from central to eastern Texas, consistent with changes in water supply pattern. We find that in normal years GRACE TWS shows strong coupling and similar characteristic time scale to surface SM, while in drier years GRACE TWS manifests stronger persistence, implying longer recovery time and prolonged water supply constraint on vegetation growth. The synergistic combination of GRACE TWS and surface SM, along with remote-sensing vegetation observations provides new insights into drought impact on vegetation–moisture relationship, and unique information regarding vegetation resilience and the recovery of hydrological drought.

Introduction

The state of Texas and surrounding areas have experienced multiple severe drought events during the last decade (NOAA 2007, 2011, Dong *et al* 2011, Combs 2012, Hoerling *et al* 2013, Long *et al* 2013). A severe hydrological drought occurred from 2011–2013 over Texas and surrounding areas, exacerbating regional water supply shortages, wildfire disturbance, and drought-induced tree mortality; it also decreased agricultural productivity and raised energy demand (Combs 2012, Scanlon *et al* 2013, Schwantes *et al* 2016). Severe and extensive drought has direct impact on both terrestrial water and carbon cycles. Vegetation

© 2017 IOP Publishing Ltd

gross primary production (GPP) from canopy photosynthesis is the primary conduit of carbon transfer between the land and atmosphere. The GPP reduction in response to declining water supply and drought stress weakens the terrestrial carbon sink (e.g. Zhao and Running, 2011, Schaefer *et al* 2012, Schwalm *et al* 2012). Thus to assess and reduce drought impact, it is essential to monitor and understand how drought disturbance influences the water supply pattern and affects vegetation productivity.

The development of a severe drought starts from changes in atmospheric processes and the deterioration of climatic water supply, which in turn affects surface soil moisture replenishment and deeper groundwater storage recharge. Drought recovery also involves the same top-to-bottom changes in each of these water storage components (e.g. Van Loon, 2015). A complete characterization and understanding of drought and its impact therefore require an assessment of terrestrial water storage (TWS) components covering the entire water column.

From 2002 to present, GRACE satellite measurements have provided regional estimates of monthly changes in TWS (Swenson *et al* 2006, Reager and Famiglietti, 2009, Famiglietti *et al* 2011) including water storage components from snow cover, surface water, soil moisture and deeper groundwater. GRACE data have been used extensively to study changes in water supply pattern (Rodell *et al* 2009, Landerer *et al* 2010, Velicogna *et al* 2012), to investigate drought and its impact (Chen *et al* 2009, 2013, Long *et al* 2013, Castle *et al* 2014, Thomas *et al* 2014, Zhao *et al* 2017), and to study water constraints on vegetation growth (Yang *et al* 2014, A *et al* 2015). Complementary to GRACE TWS observations that estimate the overall water supply condition, soil moisture (SM) retrievals from satellite microwave sensors provide enhanced delineation of plant-accessible water storage within the upper soil layers (Entekhabi *et al* 2010, Mladenova *et al* 2014, Du *et al* 2016).

Here we study how drought affects vegetation sensitivities to inter-annual changes in surface soil moisture and the overall water storage using a suite of synergistic overlapping global satellite sensor observations. We use GRACE observation of TWS as proxy of TWS conditions of the entire water column and surface soil moisture retrievals from AMSR-E/2 satellite microwave sensors as an indicator of the dynamic surface (within ~5 cm depth) SM signal. We use MODIS enhanced vegetation index (EVI), GOME-2 solar-induced fluorescence (SIF) and MODIS GPP as a proxy of vegetation growth changes. The domain of our investigation centers on the state of Texas and surrounding semiarid areas within the southwest USA; this region features water-limited vegetation growth conditions representative of the southern Great Plains and has experienced severe and persistent drought conditions in the last decade.

We first evaluate the 2011 drought condition by analyzing the corresponding water supply deficit from GRACE TWS and AMSR-E/2 SM, and the associated reduction in vegetation growth estimated from MODIS EVI, GOME-2 SIF and MODIS GPP. We then examine drought-induced changes in the temporal correlations between vegetation growth and water storage variations, in relation to plant functional types and changes in water supply pattern. We investigate how drought modulates the variability and persistence of shallow-depth surface SM and overall TWS, and its implication for vegetation-moisture relationship and drought recovery. We also evaluate the vegetation sensitivity to surface and overall water storage changes for each season in the analyzed area. We conclude on the implication of combining synergistic satellite observations to characterize drought evolution across the soil-vegetation-atmosphere system for improving understanding of vegetation sensitivity to water storage changes from surface soil and deeper groundwater sources.

Data and method

We use 131 monthly GRACE solutions from the Center for Space Research at the University of Texas (Tapley *et al* 2004), between August 2002 and December 2013. Each gravity solution consists of spherical harmonic coefficients up to degree and order 60. We replace GRACE-derived degree-2 and order-0 coefficients with those estimated from satellite laser ranging (Cheng *et al* 2013) and include degree-1 coefficients calculated following Swenson *et al* (2008). We correct GRACE solutions for the glacial isostatic adjustment (GIA) signal following A *et al* (2013). GRACE-derived TWS anomalies are calculated relative to the period from August 2002-December 2013. To reduce the random error components, we apply a Gaussian smoothing with a 400 km radius (Wahr *et al* 1998) and then generate a monthly TWS time series over a half-degree latitude-longitude grid.

For the long-term SM record, we use a consistent global surface soil moisture record derived from similar calibrated, overlapping microwave brightness temperature (T_b) retrievals from AMSR-E (Advanced Microwave Scanning Radiometer for EOS), FY3B-MWRI (Microwave Radiation Imager) and AMSR-2 (AMSR follow-on instrument onboard the JAXA GCOM-W1 satellite) sensor records (Du *et al* 2014). The SM record has global coverage and 1–3 d temporal fidelity as derived from AM orbit T_b observations, while an iterative retrieval algorithm is used with multiple T_b frequencies and polarizations to account for potential negative impacts on the soil moisture retrievals from atmosphere precipitable water vapor, open water inundation, vegetation biomass cover and surface temperature variations (Du *et al* 2014). The resulting 10.7 GHz SM retrievals are primarily

sensitive to moisture conditions within the surface (~0–2 cm depth) soil layer under low to moderate vegetation biomass cover characteristic of semiarid grassland and shrubland vegetation within the domain (Du *et al* 2016). The SM retrievals are mapped to a consistent 25 km resolution global grid and daily time step with well characterized accuracy and performance (Du *et al* 2014, 2016, Mladenova *et al* 2014).

We use three sets of satellite records to represent vegetation growth condition, including NASA EOS MODIS MOD13C2 (Collection 5) enhanced vegetation index (EVI) record (Huete *et al* 2011), MOD17A2 (Collection 5) GPP record (Zhao *et al* 2005, Zhao and Running, 2011) and GOME-2 (Global Ozone Monitoring Experiment-2) (Version 26, Level 3) 740 nm solar induced fluorescence (SIF) record (Joiner *et al* 2013). The MOD13 EVI record has been widely used to represent both vegetation state and productivity (e.g. Sims *et al* 2006, Seddon *et al* 2016). The MOD17 GPP record used for this investigation has undergone five major reprocessing improvements and has well documented global accuracy (e.g. Heinsch *et al* 2006, Turner *et al* 2006, Huntzinger *et al* 2012). Both MODIS EVI and GPP records extend from Feb 2000 to present and are produced at 1 km resolution and 8 d temporal fidelity. The GOME-2 measurement provides longest SIF record since 2007. Recent studies have shown that the flux of chlorophyll fluorescence emitted from canopy photosynthetic process is a more direct indicator of GPP (Joiner *et al* 2013, Frankenberg *et al* 2014). The SIF record is generated monthly at a spatial resolution of 0.5°. For consistency, all vegetation metrics are composited to a monthly time step at a 0.5° × 0.5° global grid. We also use the MODIS MCD12Q1 (Collection 5) land cover type product to define the vegetation distribution in the study domain (Friedl *et al* 2010).

A satellite microwave remote sensing based global record of daily landscape freeze-thaw status is used to define the annual non-frozen (NF) season for each grid cell over the domain (Kim *et al* 2011, 2014). We then treat the NF period, which spans most of the year in the study domain, as the potential growing season for evaluating vegetation-moisture relationships. We use ERA-Interim monthly 2 m height air temperature (Dee *et al* 2011) for removal of the temperature dependency on vegetation growth in the partial correlation analysis; we also include precipitation from the Global Precipitation Climatology Project (Adler *et al* 2003, Huffman *et al* 2009) to represent water inputs to the analyzed system. For consistent comparison, all datasets are processed in the same way as the GRACE data unless otherwise noted (text S1 available at stacks.iop.org/ERL/12/054006/mmedia). The GRACE processing provides regionally averaged time series but largely preserves the inter-annual variability from the finer-scale time series (text S1, figure S1).

In this study, we utilize a *z*-score standardization approach for comparison of the vegetation-moisture relationships across different spatial and temporal domains. There is both spatial and temporal variability in local climate, and therefore the same amount of water deficit may have significantly different impact on biomes at one location or time period than another (e.g. Ji and Peters, 2003, Vicente-Serrano *et al* 2013). To account for this, we apply *z*-score standardization to the time series of interest as follows:

$$z_{i,j} = \frac{x_{ij} - \overline{x}_j}{\sigma_j} \quad (1)$$

where i is the year ranging from 2002 to 2013, j is the month ranging from January to December, $\overline{x}_j$ and σ_j are the mean and standard deviation of time series x at month j (e.g. Zhao *et al* 2017). This procedure effectively removes the climatology from the original time series and normalizes the time series according to its monthly standard deviation. We generate *z*-score inter-annual time series of the satellite and ancillary data records for correlation analysis (figures 2–4).

We also utilize a 13-month temporal smoothing to reduce higher temporal frequency seasonal variations and to illustrate longer-term trends and inter-annual variability (figures 4(*c*) and (*d*)). To do this for each 13-month window, we simultaneously solve for annual, semiannual, 3-month period signals, a constant and a linear trend. We assign the sum of the constant term and the linear trend to the center point (i.e., the 7th month) of each time window. This moving average scheme yields a smoothed time series where seasonal variations are effectively removed.

To investigate the inter-annual correspondence between vegetation growth and each water storage component, we calculate the NF season partial correlations between EVI and TWS ($R_{\text{EVI-TWS}}$), EVI and SM ($R_{\text{EVI-SM}}$), SIF and TWS ($R_{\text{SIF-TWS}}$), SIF and SM ($R_{\text{SIF-SM}}$), GPP and TWS ($R_{\text{GPP-TWS}}$), and GPP and SM ($R_{\text{GPP-SM}}$) using the corresponding de-trended *z*-score time series. We de-trend the time series to obtain more conservative estimate of correlation coefficients: for each time series, a 2-segment piecewise linear trend is fitted and removed from each grid cell before we compute the correlation (online supplementary text S2). We find large trend only for GRACE TWS during 2010–2013. The de-trending procedure does not change the spatial pattern of vegetation-moisture correlation, but generally leads to more conservative estimates of correlation strength (online supplementary text S2, figure S2). Vegetation growth in the semiarid Texas area is water-constrained. We use partial correlation to remove the possible impact of temperature on growth, i.e. we calculate the linear regression between temperature and each of the analyzed variables, remove the linear fit and then use the residual time series to compute correlation coefficients (e.g. Piao *et al* 2014).

To evaluate the memory effect and persistence in water storage components, we compute autocorrelation

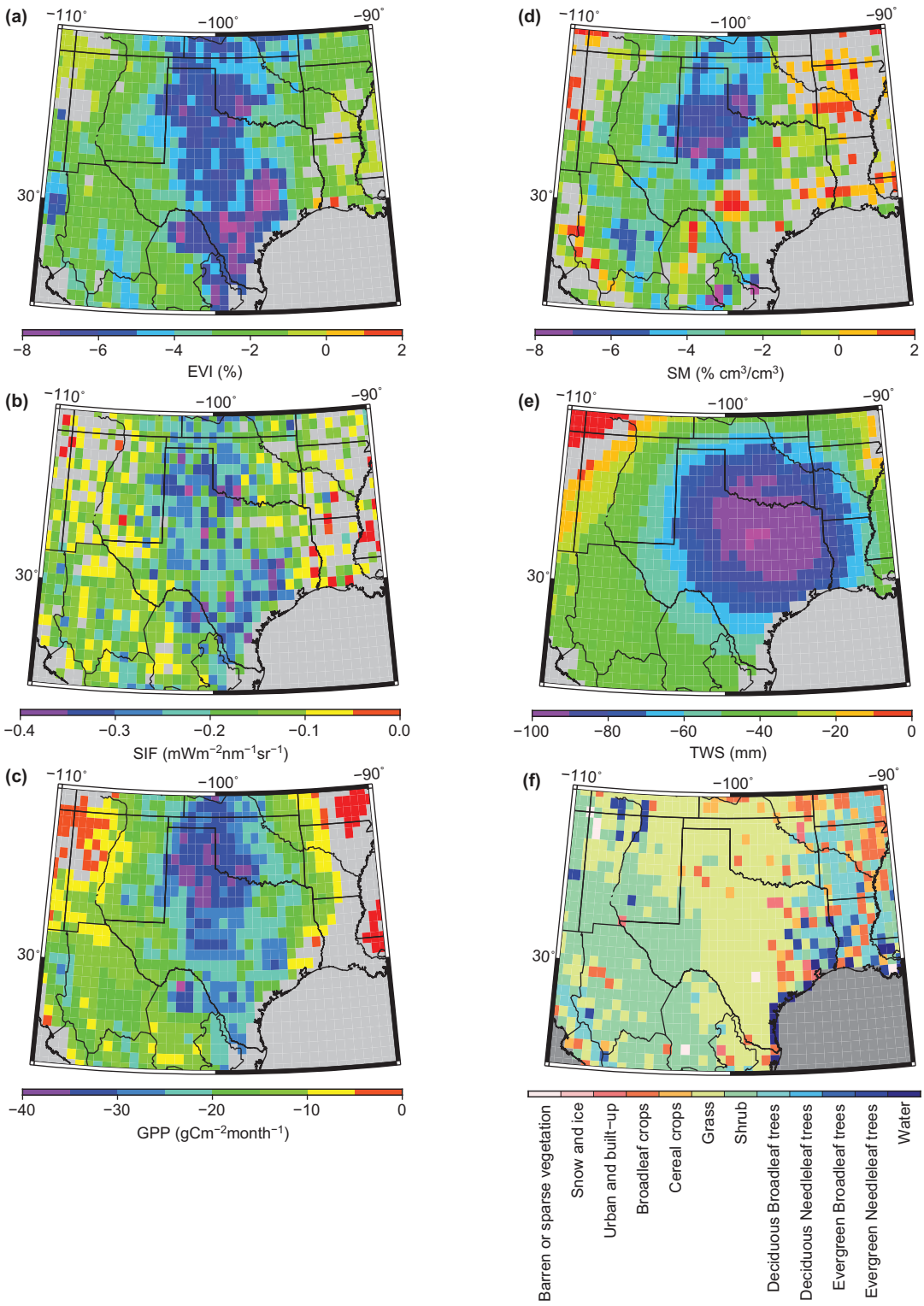

Figure 1. The 2011 mean anomalies of (*a*) EVI in %, (*b*) SIF in $mWm^{-2}nm^{-1}sr^{-1}$, (*c*) GPP in $gCm^{-2}month^{-1}$, (*d*) SM in % cm^3cm^{-3} and (*e*) TWS in mm, relative to the 2007–2010 (pre-drought) means. Only results significant up to $1-\sigma$ are shown. (*f*) Land cover type in the analyzed area. Results (except for TWS) are shown at a 0.5° grid without Gaussian spatial averaging.

functions for the *z*-score time series of SM and TWS. Again we de-trend the time series to obtain more conservative estimate of the correlation coefficients (online supplementary text S2, figure S2). We define a characteristic time scale for each time series data record as the lag time when the amplitude of the autocorrelation function decreases to *1/e*.

Results

We show in figures 1(*a*)–(*e*) the annual anomalies (up to 1-σ) of EVI, SIF, GPP, SM and TWS in 2011 relative to the pre-drought common period of 2007–2010. We find strong spatial agreement among EVI, SIF and GPP observations, all indicating vegetation growth

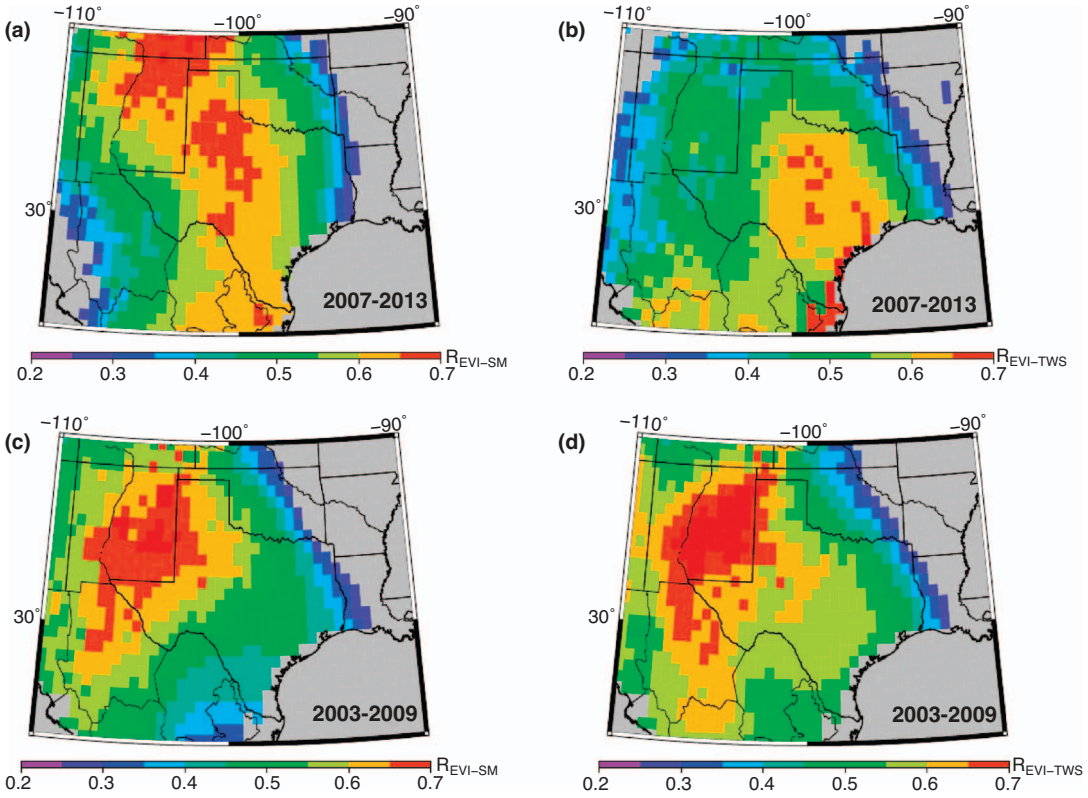

Figure 2. Partial correlation coefficients (significant up to 98% confidence level) for (*a*) EVI and SM ($R_{\text{EVI-SM}}$), (*b*) EVI and TWS ($R_{\text{EVI-TWS}}$) for the NF seasons during the 7 yr period of 2007–2013 including a severe hydrological drought; panels (*c*) and (*d*) show the same correlation coefficients for the NF seasons during the relatively normal years of 2003–2009.

reduction in the analyzed domain, with the largest decrease occurring in the grassland region (figures 1 (*a*)–(*c*), (*f*)). SIF results show notable speckling compared to EVI and GPP, likely due to its high retrieval noise in low productivity grassland region. Both SM and TWS observations capture the deteriorated water supply condition in 2011, where surface SM shows significant decrease in the northern grasslands and the overall TWS shows large deficit in the grassland and forest areas from central to eastern Texas (figures 1(*d*)–(*f*)).

Figures 2(*a*) and (*b*) show the vegetation-moisture correlations calculated using the de-trended EVI, TWS and SM *z*-score time series during the common period of 2007–2013; here we consider only areas where the partial correlation coefficient is statistically significant at more than 98% confidence level ($p < 0.02$). We find strong correlations over majority of the analyzed domain for each pair of vegetation-moisture observables. EVI shows strong correspondence with SM changes in the central grassland band (figure 2(*a*)), same area where we observe largest EVI reduction during the 2011 drought (figure 1(*a*)). The EVI correlation with TWS is strongest in the grassland and forest area spanning from central to eastern Texas (figure 2(*b*)), same area where we observe largest TWS deficit in 2011 (figure 1(*e*)). To illustrate vegetation-moisture relationships prior to the hydrological drought, we show in figure 2(*c*) and (*d*) correlations calculated using time series from 2003–2009; this period has a 7 yr duration (same duration as for 2007–2013) and samples the pre-drought condition. We find congruent EVI responses to changes in surface SM and to overall TWS. Both correlations are strongest in the drier shrubland and grassland to the west, and are weaker or insignificant in the moist east, consistent with the annual precipitation gradient over the analyzed domain (figure S6).

Figure 3 shows the same comparison but using SIF and GPP as the vegetation metrics. We find the same GPP correlations as those using EVI during 2003–2009 (figures 3(*e*) and (*f*). Correlations involving SIF are not shown for this pre-drought period due to its short record length. During 2007–2013, $R_{\text{SIF-SM}}$ and $R_{\text{SIF-TWS}}$ show strong agreement with those using EVI (figures 3(*a*)–(*b*)). $R_{\text{GPP-SM}}$ is strongest in the center and western portion of the analyzed domain (figure 3 (*c*)). $R_{\text{GPP-TWS}}$ is significant and of same magnitude over most of the analyzed domain (figure 3(*d*)).

The 2007–2013 period includes relatively normal years before the drought. When we focus on a shorter 2010–2013 period (online supplementary text S3, figure S3) covering exclusively the onset, peak and recovery of the hydrological drought, we find the same spatial pattern for $R_{\text{EVI-SM}}$, $R_{\text{EVI-TWS}}$, $R_{\text{SIF-SM}}$, and $R_{\text{SIF-TWS}}$ as those shown in figures 2 and 3, but with a slightly larger magnitude. The GPP correlations are now in agreement with those using EVI and SIF, with stronger $R_{\text{GPP-SM}}$ in the grassland region and significant $R_{\text{GPP-TWS}}$ in the center and east.

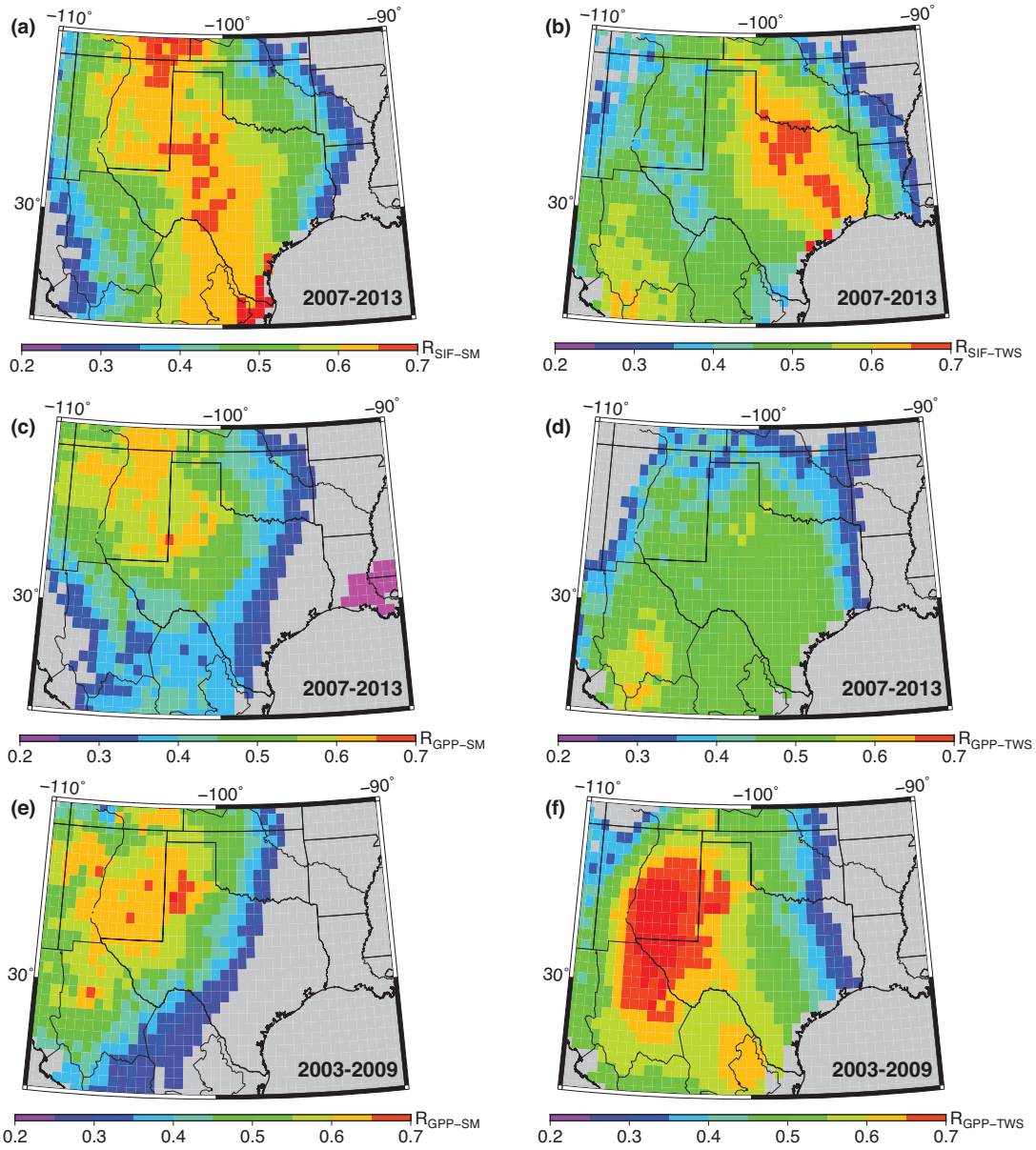

Figure 3. Similar to figure 2, panels (*a*)−(*d*) show the partial correlation coefficients (significant up to 98% confidence level) for $R_{SIF\text{-}SM}$, $R_{SIF\text{-}TWS}$, $R_{GPP\text{-}SM}$, and $R_{GPP\text{-}TWS}$, respectively, using the NF seasons during 2007–2013. Panels (*e*) and (*f*) show $R_{GPP\text{-}SM}$, and $R_{GPP\text{-}TWS}$ for the NF seasons during 2003–2009.

As shown in figures 2 and 3, vegetation growth shows different responses to surface SM and overall TWS changes since the initiation of the hydrological drought, and we find a transition in the spatial pattern of vegetation-moisture correspondence: vegetation sensitivity to SM variations weakens slightly in the shrub-dominated west and strengthens in the central grassland band; and regions with strong TWS dependency has experienced a shift from the west to the grassland and forest area in the center and east.

Notably in the western portion of the domain, vegetation growth shows small or insignificant correlation with TWS during the drought period (figure 2(*b*), figures 3(*b*) and (*d*), figures S3(*d*)–(*f*)) while the correlation with SM is still significant. Indeed, drought disturbance influences SM and TWS differently, which would in turn impact vegetation sensitivities to SM and TWS. Before 2010, TWS variation is significantly correlated with surface SM changes over the entire domain (figure 4(*a*)), implying that in the normal years shallow-depth SM changes, that are directly accessible to plant, dominate overall TWS variability. After 2010, the SM-TWS correlation weakens significantly in the western shrub-dominated area (figure 4(*b*)), suggesting a decoupling between shallow-depth and overall water variations. To analyze the changes in this shrub-dominated area, we outline a 400 km-radius sub-region centered at (32°N, 104°W) (figure 4(*a*)), and we show the time series of each observable averaged in the sub-region and filtered for seasonal dependence using a 13 m window (figures 4 (*c*) and (*d*)). Vegetation growth shows congruent correspondence with both SM and TWS before 2010. Since mid-to-late 2010, SM and TWS decline rapidly,

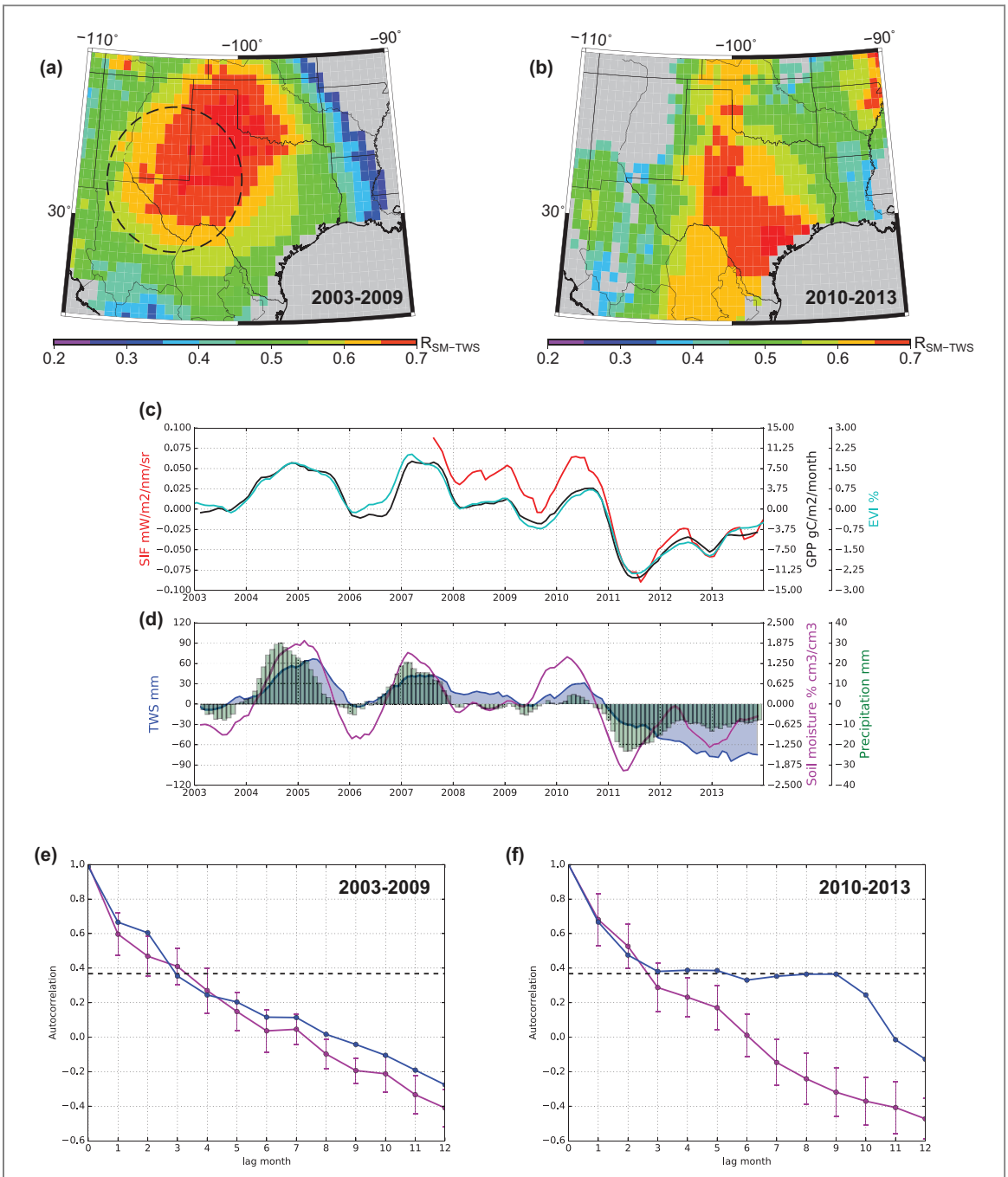

Figure 4. Panels (*a*) and (*b*) show partial correlation coefficients between SM and TWS ($R_{\text{SM-TWS}}$) during 2003–2009 and 2010–2013, respectively. The dashed circle in panel (*a*) outlines a 400 km-radius area centered at (32°N, 104°W), where we show anomalies of EVI (cyan), SIF (red), GPP (black) in panel (*c*); and SM (magenta), TWS (blue), and precipitation (green) in panel (*d*), filtered for the seasonal dependence using a 13 month window. Panels (*e*) and (*f*) show autocorrelation functions of TWS (blue) and SM (magenta) during 2003–2009 and 2010–2013, respectively. The solid lines show averaged results over the circle area. The error bar for SM is estimated using the standard deviation of autocorrelation results at each 0.5° × 0.5° grid cell within the 400 km area. The black dashed lines show an e-folding reduction in the autocorrelation, which is used to define the characteristic time scale of the time series.

followed by reduction in EVI, SIF and GPP; vegetation metrics start to show greater sensitivity to SM than TWS. After 2011, we observe episodic increases in growth associated with precipitation-driven surface wetting while TWS shows a consistent declining trend through the 2010–2013 record. Correlations computed using the de-trended time series before and after 2010 also show a decrease in $R_{\text{EVI-TWS}}$ from 0.66 ($p < 0.001$) to 0.36 ($p = 0.03$), while $R_{\text{EVI-SM}}$ is relatively stable (from 0.63 to 0.61; $p < 0.001$) (See also Text S3).

In this shrub-dominated region, we attribute the contrasting response of vegetation to SM and TWS to different drought impacts on the characteristic time scale and persistence of each hydrological component. As shown in figure 4(*d*), SM exhibits similar sensitivity to precipitation through the entire analyzed period, consistent with dynamic wetting and drying of surface SM. In contrast, TWS is less sensitive to precipitation during the hydrological drought than the earlier record. This implies that the persistence or memory effect in TWS is enhanced during the

exceptional drought. To investigate this further, we compute the autocorrelation functions using the de-trended TWS and SM *z*-scores before and after 2010. TWS and SM show a similar autocorrelation function for 2003–2009 (figure 4(*e*)). If we define a characteristic time scale using the lag time when the amplitude of the autocorrelation decreases to 0.368 (or *1/e*), we find that TWS and SM have a time scale of 2.9 and 3.2 m, respectively, implying that the persistence of TWS and SM both extend up to about 3 m over the initial record. During the 2010–2013 period, however, we find a notable difference between the SM and TWS autocorrelations: the SM shows a time scale of 2.7 m, while the TWS shows stronger autocorrelation, especially at the 7–9 m time scale (figure 4(*f*)). The longer TWS time scale during the hydrological drought likely reflects temporal variability in deeper groundwater storage that is less accessible to local shrub growth, consistent with previous studies based on a multi-scalar drought index (e.g. Vicente-Serrano *et al* 2010, 2013, Wang *et al* 2015). We have also compared SM and TWS autocorrelations before and after drought in the central grassland band; there the SM and TWS time scales are less sensitive to drought, and TWS generally shows stronger persistence than SM (~4–5 m for TWS, ~3 m for SM) through the entire period. In our analysis, autocorrelation functions are calculated during 2003–2009 and the drier 2010–2013, involving different sample sizes. We have tested the sensitivity of the autocorrelation analysis to the sample size and find that it does not affect our results (online supplementary text S4, figure S4).

To evaluate possible seasonal dependency of the vegetation-moisture relationships in the analyzed domain, we have examined the annual *z*-score time series of EVI, SIF, GPP, TWS and SM averaged for each of the four seasons (online supplementary figure S5). Despite the occurrence of 2011 drought, we find consistent seasonal vegetation-moisture correspondence through the entire period: vegetation sensitivity to water is strong from spring to fall, and weaker only in the winter months. Indeed, in semiarid/arid climate zones, seasonal temperature and energy constraints on vegetation growth are less important than available water supply as the main driver of vegetation productivity.

Discussion

This study focuses on the state of Texas and surrounding semiarid grassland and shrubland areas. This region features an east-west gradient in mean annual precipitation with generally drier conditions in the western portion of the domain. Some of the areas in the west receive less than 400 mm of annual precipitation, contrasting with up to 1000 mm of annual rainfall for some eastern areas of the domain. We find that this climate gradient largely determines the regional pattern of vegetation-moisture relationships in normal years (before the 2011 hydrological drought). In the drier portion of the domain, variations in vegetation productivity are strongly correlated with changes in both surface soil moisture and total water storage, whereas in wetter areas, vegetation dependency on water supply is less significant (figures 2(*c*) and (*d*), figures 3(*e*) and (*f*)). This general relationship is consistent with previous studies based on water supply pattern at both regional scale and site level (e.g. Nemani, 2003, Huxman *et al* 2004).

However we find that drought disturbance affects this regional pattern of vegetation-moisture relationships, depending on the underlying plant functional types. In the central grassland band, vegetation growth under drought manifests enhanced sensitivity to surface SM variations (figures 2, 3 and S3), implying strong susceptibility of semiarid grassland to drought disturbance (Knapp and Smith, 2001, Moran *et al* 2014). This is also consistent with the larger SIF, EVI and GPP reductions observed in the grassland area during the 2011 drought (figures 1(*a*)–(*c*)). On the other hand, this enhanced sensitivity to SM variations also leads to rapid recovery of vegetation growth following the replenishment of surface SM after the drought disturbance, implying strong drought resilience for the grassland.

In the shrub-dominated west, vegetation growth under drought show slightly smaller but significant correlation with surface SM, and the sensitivity to TWS weakens significantly compared to the earlier record (figures 2, 3 and S3). It is likely that in this area, the TWS variations during the exceptional drought occur at a depth beyond the local plant root zone. The 2011 hydrological drought in Texas is reported to have caused widespread mortality in woody vegetation (Schwantes *et al* 2016), which might also weaken regional vegetation-moisture correspondence.

In the eastern Texas, plant water sensitivity transitions from low to strong after the hydrological drought. This is due to the deteriorated water supply condition caused by the exceptional TWS anomaly (figure 1(*e*)). We also find stronger vegetation sensitivity to changes in overall TWS than surface SM in this region. This may be attributed to deeper rooting systems associated with the abundant tree coverage (e.g. Schenk and Jackson, 2002) and also indicates that the recovery of vegetation growth in this region relies on the water replenishment in the entire soil column, rather than only in the surface layer.

The differential vegetation drought response is also linked to drought-induced changes in the hydrological cycle. The GRACE TWS signal detects water storage changes over the entire water column, extending from surface to deeper groundwater sources, with each storage component featuring different characteristic time scales of variability

(Vicente-Serrano *et al* 2010, 2013, Wang *et al* 2015, Zhao *et al* 2017). The time scale estimate derived from autocorrelation measures the inertia of the time series, or how long an anomaly can persist. Our results show that an exceptional drought disturbance can modulate this inertia. The longer TWS time scale during the hydrological drought indicates that larger or more persistent water replenishment are required to alter the deficit status of water supply, which implies a longer recovery time and prolonged constraint on vegetation growth following a major drought.

Previous studies have suggested that an increase in temporal autocorrelation and decrease in recovery rate may indicate a system approaching an ecological tipping point (e.g. Dakos *et al* 2008, Scheffer *et al* 2009, Seddon *et al* 2016). Our results demonstrate that the GRACE TWS time series can be used to evaluate changes in the characteristic time scale of the underlying water supply variations influencing vegetation growth, and the slowing recovery rate in TWS may serve as a warning signal to detect critical transitions in the terrestrial hydrological cycle affecting ecosystem service.

Natural grassland and shrubland in semiarid and arid climate zones have drought tolerant adaptations, including relatively deep rooting systems allowing plant access to groundwater to sustain productivity under dry surface SM and atmosphere conditions (McDowell *et al* 2008). It is, however, a challenge to understand how vegetation under drought stress responds to changes in hydrological components at different soil depths and with varying temporal signatures, which has important implications for drought resilience associated with each plant specie (Wang *et al* 2007, Vicente-Serrano *et al* 2013, Zhao *et al* 2017). This study utilizes AMSR-E/2 SM and GRACE TWS to provide respectively estimates of shallow-depth and overall water supply influencing vegetation growth. Subsequent partitioning of the GRACE TWS is needed to fully distinguish water supply variations within the entire soil column. Future studies may benefit by incorporating lower frequency (e.g. L-band) satellite microwave remote sensing to enable enhanced delineation of surface to root zone soil moisture changes affecting vegetation productivity (Entekhabi *et al* 2014).

Conclusions

We use synergistic overlapping satellite environmental data records to investigate recent drought related impacts on terrestrial water storage and ecosystem productivity in the state of Texas and surrounding semi-arid areas over the past decade (2003–2013). The satellite data examined included bulk terrestrial water storage (TWS) from GRACE, surface soil moisture (SM) from AMSR-E/2, enhanced vegetation index (EVI) and vegetation gross primary production (GPP) from MODIS, and solar-induced fluorescence (SIF) from GOME-2, with each of them featuring unique spatial and temporal signature. We expect that the same methodology of aggregation and normalization (Text S1, figure S1) adopted in this work may facilitate future dataset inter-comparison using other remote-sensing products including the SMAP data (Entekhabi *et al* 2014).

We find both SM and TWS capture water supply constraints to vegetation growth, distinguishing relatively rapid SM wetting and drying of the surface soil layer from TWS variations including larger and deeper groundwater sources. In relatively normal years, vegetation growth shows congruent sensitivity to changes in surface and overall water storage, and the spatial pattern of vegetation-moisture relationship follows the regional gradient in mean annual precipitation. Following the hydrological drought, vegetation growth in the central grassland shows enhanced sensitivity to SM variations. Vegetation sensitivity to TWS variations weakens in the western shrubland, and strengthens in the grassland and forest area spanning from center to the east. Together these results show contrasting vegetation sensitivity to surface SM and total water storage in the drier period, implying different drought susceptibility and resilience associated with each plant functional type.

In the analyzed region, the inter-annual variability of total water storage is closely associated with changes in surface soil moisture, while the relationship between TWS and SM diverges under drought conditions. We find that in relatively normal years TWS shows strong coupling and similar characteristic time scale to surface SM, while TWS manifests longer temporal variability and stronger persistence than surface SM under severe drought, implying longer recovery time and sustained water constraint to plant growth.

The ongoing SMAP mission and planned GRACE-FO/2 mission will provide enhanced observations of surface to root zone SM and TWS, including model enhanced assessment of soil moisture related water supply constraints affecting GPP (Kimball *et al* 2015). The current array of complimentary satellite Earth observations provides new opportunities for global drought monitoring and better understanding of hydrological and ecosystem interactions.

Acknowledgments

This work was performed at UCI and JPL-Caltech. It was partially supported by the NASA's Terrestrial Hydrology, IDS, MEASURES Programs, Gordon and Betty Moore Foundation (GBMF3269). Data used in this manuscript are available upon request from the authors. We thank the editor and the two reviewers for their careful reviews.

References

A G, Wahr J and Zhong S 2013 Computations of the viscoelastic response of a 3-D compressible Earth to surface loading: an application to glacial isostatic adjustment in Antarctica and Canada *Geophys. J. Int.* **192** 557–72

A G, Velicogna I, Kimball J S and Kim Y 2015 Impact of changes in GRACE derived terrestrial water storage on vegetation growth in Eurasia *Environ. Res. Lett.* **10** 124024

Adler R F *et al* 2003 The version-2 global precipitation climatology project (GPCP) monthly precipitation analysis (1979–present) *J. Hydrometeorol.* **4** 1147–67

Castle S L, Thomas B F, Reager J T, Rodell M, Swenson S C and Famiglietti J S 2014 Groundwater depletion during drought threatens future water security of the Colorado River Basin *Geophys. Res. Lett.* **41** 5904–11

Chen J L, Wilson C R, Blankenship D and Tapley B D 2009 Accelerated Antarctic ice loss from satellite gravity measurements *Nat. Geosci.* **2** 859–62

Chen Y, Velicogna I, Famiglietti J S and Randerson J T 2013 Satellite observations of terrestrial water storage provide early warning information about drought and fire season severity in the Amazon *J. Geophys. Res. Biogeosci.* **118** 495–504

Cheng M, Tapley B D and Ries J C 2013 Deceleration in the Earth's oblateness *J. Geophys. Res. Solid Earth* **118** 740–7

Combs S 2012 The Impact of the 2011 drought and beyond. Special Report Publication# 96–1704 *Texas Comptrol. Public Accounts* 1–16

Dakos V, Scheffer M, van Nes E H, Brovkin V, Petoukhov V and Held H 2008 Slowing down as an early warning signal for abrupt climate change *Proc. Natl Acad. Sci. USA* **105** 14308–12

Dee D P *et al* 2011 The ERA-interim reanalysis: configuration and performance of the data assimilation system *Q. J. R. Meteorol. Soc.* **137** 553–97

Dong X *et al* 2011 Investigation of the 2006 drought and 2007 flood extremes at the Southern Great Plains through an integrative analysis of observations *J. Geophys. Res. Atmos.* **116** D03204

Du J, Kimball J, Shi J, Jones L, Wu S, Sun R and Yang H 2014 Inter-calibration of satellite passive microwave land observations from AMSR-E and AMSR2 using overlapping FY3B-MWRI sensor measurements *Remote Sens.* **6** 8594–616

Du J, Kimball J S and Jones L A 2016 Passive microwave remote sensing of soil moisture based on dynamic vegetation scattering properties for AMSR-E *IEEE Trans. Geosci. Remote Sens.* **54** 597–608

Entekhabi D *et al* 2010 The soil moisture active passive (SMAP) mission *Proc. IEEE* **98** 704–16

Entekhabi D *et al* 2014 JPL Publication 400–1567 *SMAP Handbook* (Pasadena, CA: Jet Propulsion Laboratory) p 182 (https://smap.jpl.nasa.gov/files/smap2/SMAP_Handbook_FINAL_1_JULY_2014_Web.pdf)

Famiglietti J S, Lo M, Ho S L, Bethune J, Anderson K J, Syed T H, Swenson S C, de Linage C R and Rodell M 2011 Satellites measure recent rates of groundwater depletion in California's Central Valley *Geophys. Res. Lett.* **38** L03403

Frankenberg C, O'Dell C, Berry J, Guanter L, Joiner J, Köhler P, Pollock R and Taylor T E 2014 Prospects for chlorophyll fluorescence remote sensing from the orbiting carbon observatory-2 *Remote Sens. Environ.* **147** 1–12

Friedl M A, Sulla-Menashe D, Tan B, Schneider A, Ramankutty N, Sibley A and Huang X 2010 MODIS collection 5 global land cover: algorithm refinements and characterization of new datasets *Remote Sens. Environ.* **114** 168–82

Heinsch F A *et al* 2006 Evaluation of remote sensing based terrestrial productivity from MODIS using regional tower eddy flux network observations *IEEE Trans. Geosci. Remote Sens.* **44** 1908–25

Hoerling M, Kumar A, Dole R, Nielsen-Gammon J W, Eischeid J, Perlwitz J, Quan X W, Zhang T, Pegion P and Chen M 2013 Anatomy of an extreme event *J. Clim.* **26** 2811–32

Huete A, Didan K, Van Leeuwen W, Miura T and Glenn E 2011 MODIS vegetation indices *Land Remote Sensing and Global Environmental Change* ed B Ramachandran, C O Justice and M J Abrams vol **11** (New York: Springer) pp 579–602

Huffman G J, Adler R F, Bolvin D T and Gu G 2009 Improving the global precipitation record: GPCP version 2.1 *Geophys. Res. Lett.* **36** 1–5

Huntzinger D N *et al* 2012 North American Carbon Program (NACP) regional interim synthesis: terrestrial biospheric model intercomparison *Ecol. Modell.* **232** 144–57

Huxman T E *et al* 2004 Convergence across biomes to a common rain-use efficiency *Nature* **429** 651–4

Ji L and Peters A J 2003 Assessing vegetation response to drought in the northern Great Plains using vegetation and drought indices *Remote Sens. Environ.* **87** 85–98

Joiner J, Guanter L, Lindstrot R, Voigt M, Vasilkov A P, Middleton E M, Huemmrich K F, Yoshida Y and Frankenberg C 2013 Global monitoring of terrestrial chlorophyll fluorescence from moderate spectral resolution near-infrared satellite measurements: methodology, simulations, and application to GOME-2 *Atmos. Meas. Tech. Discuss.* **6** 3883–930

Kim Y, Kimball J S, Mcdonald K C and Glassy J 2011 Developing a global data record of daily landscape freeze/thaw status using satellite passive microwave remote sensing *IEEE Trans. Geosci. Remote Sens.* **49** 949–60

Kim Y, Kimball J S, Didan K and Henebry G M 2014 Response of vegetation growth and productivity to spring climate indicators in the conterminous United States derived from satellite remote sensing data fusion *Agric. For. Meteorol.* **194** 132–43

Kimball J S, Jones L A, Glassy J, Stavros E N, Madani N, Reichle R H, Jackson T and Colliander A 2015 Soil Moisture Active Passive (SMAP) Project Calibration and Validation for the L4_C Beta-Release Data Product, *NASA/TM–2015–104606*, 42, 37 pp

Knapp A K and Smith M D 2001 Variation among biomes in temporal dynamics of aboveground primary production *Science* **291** 481–4

Landerer F W, Dickey J O and Güntner A 2010 Terrestrial water budget of the Eurasian pan-Arctic from GRACE satellite measurements during 2003–2009 *J. Geophys. Res.* **115** D23115

Long D, Scanlon B R, Longuevergne L, Sun A Y, Fernando D N and Save H 2013 GRACE satellite monitoring of large depletion in water storage in response to the 2011 drought in Texas *Geophys. Res. Lett.* **40** 3395–401

McDowell N *et al* 2008 Mechanisms of plant survival and mortality during drought: why do some plants survive while others succumb to drought? *New Phytol.* **178** 719–39

Mladenova I E *et al* 2014 Remote monitoring of soil moisture using passive microwave-based techniques—theoretical basis and overview of selected algorithms for AMSR-E *Remote Sens. Environ.* **144** 197–213

Moran M S *et al* 2014 Functional response of US grasslands to the early 21st-century drought *Ecology* **95** 2121–33

Nemani R R 2003 Climate-driven increases in global terrestrial net primary production from 1982 to 1999 *Science* **300** 1560–3

NOAA 2007 *State of the Climate: Drought for Annual 2006*

NOAA 2011 *State of the Climate: Drought for Annual 2010*

Piao S *et al* 2014 Evidence for a weakening relationship between interannual temperature variability and northern vegetation activity *Nat. Commun.* **5** 5018

Reager J T and Famiglietti J S 2009 Global terrestrial water storage capacity and flood potential using GRACE *Geophys. Res. Lett.* **36** L23402

Rodell M, Velicogna I and Famiglietti J S 2009 Satellite-based estimates of groundwater depletion in India *Nature* **460** 999–1002

Scanlon B R, Duncan I and Reedy R C 2013 Drought and the water–energy nexus in Texas *Environ. Res. Lett.* **8** 045033

Schaefer K *et al* 2012 A model-data comparison of gross primary productivity: results from the north American carbon program site synthesis *J. Geophys. Res. Biogeosci.* **117** 1–15
Scheffer M, Bascompte J, Brock W A, Brovkin V, Carpenter S R, Dakos V, Held H, van Nes E H, Rietkerk M and Sugihara G 2009 Early-warning signals for critical transitions *Nature* **461** 53–9
Schenk H J and Jackson R B 2002 Rooting depths, lateral root spreads and belowground aboveground allometries of plants in water limited ecosystems *J. Ecol.* **90** 480–94
Schwalm C R, Williams C A, Schaefer K, Baldocchi D, Black T A, Goldstein A H, Law B E, Oechel W C, Paw U K T and Scott R L 2012 Reduction in carbon uptake during turn of the century drought in western North America *Nat. Geosci.* **5** 551–6
Schwantes A M, Swenson J J and Jackson R B 2016 Quantifying drought-induced tree mortality in the open canopy woodlands of central Texas *Remote Sens. Environ.* **181** 54–64
Seddon A W R, Macias-Fauria M, Long P R, Benz D and Willis K J 2016 Sensitivity of global terrestrial ecosystems to climate variability *Nature* **531** 229–32
Sims D A *et al* 2006 On the use of MODIS EVI to assess gross primary productivity of North American ecosystems *J. Geophys. Res. Biogeosci.* **111** 1–16
Swenson S, Yeh P J-F, Wahr J and Famiglietti J 2006 A comparison of terrestrial water storage variations from GRACE with *in situ* measurements from Illinois *Geophys. Res. Lett.* **33** L16401
Swenson S, Chambers D and Wahr J 2008 Estimating geocenter variations from a combination of GRACE and ocean model output *J. Geophys. Res.* **113** B08410
Tapley B D, Bettadpur S, Ries J C, Thompson P F and Watkins M M 2004 GRACE measurements of mass variability in the Earth system *Science* **305** 503–5
Thomas A C, Reager J T, Famiglietti J S and Rodell M 2014 A GRACE-based water storage deficit approach for hydrological drought characterization *Geophys. Res. Lett.* **41** 1537–45
Turner D P *et al* 2006 Evaluation of MODIS NPP and GPP products across multiple biomes *Remote Sens. Environ.* **102** 282–92
Van Loon A F 2015 Hydrological drought explained *Wiley Interdiscip. Rev. Water* **2** 359–92
Velicogna I, Tong J, Zhang T and Kimball J S 2012 Increasing subsurface water storage in discontinuous permafrost areas of the Lena River basin, Eurasia, detected from GRACE *Geophys. Res. Lett.* **39** L09403
Vicente-Serrano S M, Beguería S and López-Moreno J I 2010 A multiscalar drought index sensitive to global warming: the standardized precipitation evapotranspiration index *J. Clim.* **23** 1696–718
Vicente-Serrano S M *et al* 2013 Response of vegetation to drought time-scales across global land biomes *Proc. Natl Acad. Sci. USA* **110** 52–7
Wahr J, Molenaar M and Bryan F 1998 Time variability of the Earth's gravity field: hydrological and oceanic effects and their possible detection using GRACE *J. Geophys. Res.* **103** 30205–229
Wang H, Rogers J C and Munroe D K 2015 Commonly used drought indices as indicators of soil moisture in China *J. Hydrometeorol.* **16** 1397–408
Wang X, Xie H, Guan H and Zhou X 2007 Different responses of MODIS-derived NDVI to root-zone soil moisture in semi-arid and humid regions *J. Hydrol.* **340** 12–24
Yang Y, Long D, Guan H, Scanlon B R, Simmons C T, Jiang L and Xu X 2014 GRACE satellite observed hydrological controls on interannual and seasonal variability in surface greenness over mainland Australia *J. Geophys. Res. Biogeosci.* **119** 2245–60
Zhao M and Running S W 2011 Drought-induced reduction in global terrestrial net primary production from 2000 through 2009 *Science* **333** 1093–3
Zhao M, Heinsch F A, Nemani R R and Running S W 2005 Improvements of the MODIS terrestrial gross and net primary production global data set *Remote Sens. Environ.* **95** 164–76
Zhao M, Velicogna G A I and Kimball J 2017 Satellite observations of regional drought severity in the continental US using GRACE-based terrestrial water storage changes *J. Clim.* submitted